PNAS
www.pnas.org

Supplementary Information for

Seipin accumulates and traps diacylglycerols and triglycerides in its ring-like structure.

Valeria Zoni, Rasha Khaddaj, Ivan Lukmantara, Wataru Shinoda, Hongyuan Yang, Roger Schneiter and Stefano Vanni

Stefano Vanni
Email: stefano.vanni@unifr.ch

This PDF file includes:

Supplementary Information Text

Computational Details

Molecular dynamics (MD) simulations. All MD simulations were performed using the software LAMMPS(1) in combination with the Shinoda-Devane-Klein (SDK)(2–6) and the Surface Property fItting Coarse grAining (SPICA) force field(7) for proteins (https://www.spica-ff.org) based on the previous parameterization of the individual amino acids(8). Combination rules were used to derive non-bonded interactions of TG (triolein in our simulations) and DG (dioleylglycerol) with the protein. Initial configurations and input files were obtained through conversion of atomistic snapshots using the setup lammps (https://www.spica-ff.org/index.html) or CG-it (https://github.com/CG-it/) tools and in-house scripts.
In the simulations, temperature and pressure were controlled via a Nosé-Hoover thermostat(9) and barostat (10–12). Target temperature was 310K and average pressure was 1 atm. The lateral xy dimensions were coupled, while the z dimension was allowed to fluctuate independently. Temperature was dumped every 0.5 ps, while pressure every 5 ps. Linear momentum was removed every 1 timesteps. Van der Waals and electrostatic interactions were truncated at 1.5 nm. Long-range electrostatics beyond this cutoff were computed using the particle-particle-particle-mesh (PPPM) solver, with an RMS force error of 10-5 kcal mol-1 Å-1, order 3 and a grid size of 16, 16, and 18 Å in the x, y, and z directions, respectively. A time step of 10 fs was used, except for simulations without the protein in DOPC/TG bilayers, where a timestep of 20 fs was used. An initial equilibration was carried out by performing energy minimization, followed by a short NVT run of 100 ps and a short NPT run of 100 ps.
In the simulations containing only helices (both WT seipin, scrambled seipin, 4polarL and KALP21), positional restraints along the x and y direction were used in order to preserve the ring structure, with a force constant of 10 kcal mol-1 Å-2.

MD systems setup. To build the model of the protein used in this work, the structure of the luminal portion of the human seipin (ID:6DS5)(13) was taken from RCSB PDB. Furthermore, our model includes the transmembrane (TM) domains of the protein (two per monomer), and the loops connecting the TM domains with the luminal domains. To build these domains, we first modelled the TM domains (residues 27-47 and 243-263) as fully folded alpha-helices using VMD(14). We next positioned the TM helices above the last residues solved in the crystal structure using Packmol(15). From this configuration we modelled the loops connecting the TM domains and the luminal domains using the MODELLER tool ModLoop(16). We also added 5-6 residues (residues 21-26, 263-269) on the N- and C- terminus of the protein to improve the overall stability of the model. Overall, our final model consists of the undecameric oligomer comprising the TM helices, the luminal portion and the loops connecting them (residues from 21 to 269).
This structure was embedded in a dioleoyl–phosphatidylcholine (DOPC) bilayer using CHARMM-GUI(23) and equilibrated with 10 ns all-atom MD simulations. The final coordinates were converted to CG and used as starting point for the CG simulations. In systems containing only the luminal part of the protein, the cryo-EM structure was used as a starting point.
In systems containing only the TM helices, the same approach described above was used, but the positioned helices were not connected to the rest of the protein.
In all cases, the proteins were converted to CG and an elastic network with a cutoff of 0.9 nm for the intramolecular elastic bond and a force constant of 1.195 kcal mol-1 Å-2 was used to keep the secondary structure fixed.
In order to study the dissolution of TG blisters upon protein removal, we selected the coordinates of equilibrated simulations containing seipin and we subsequently removed all the molecules outside a radius of 8 nm from the center of the protein. In the systems “without seipin”, the protein was also removed.
For the creation of mutants, all atom structures of the entire protein, helical portion or the luminal part were modified using the tool CHARMM-GUI PDB reader(17, 18). The structures were then converted to coarse grained as explained above and inserted in bilayers upon alignment with the

WT structure (entire, only helices or only luminal, depending on the case). A list of mutants and of the bilayer composition used in this study is reported in Table S1 and S2. For the creation of the scrambled helices, a random number was assigned to each amino acid of TM1 or TM2 separately and the amino acids were ranked by their newly assigned number in order to change their sequence. The final sequence of the scrambled helices is reported in Table S1.
All the systems were neutralized and ionized to a concentration of 0.15 mol/L using the GROMACS(19) tool genion. Multiple independent replicas were run and details of the systems are reported in Table S2.

Simulation analyses. The accumulation of DG/TG/PA(1-palmitoyl-2-oleoyl-glycerophosphate) /PE(dioleoyl–phosphatidylethanolamine) (lipid) molecules over time in seipin proximity was computed by summing the number of lipid molecules in annuli with a radius <=8 nm, with the exception of Figure S3 and S4 for which a radius of 6 nm was used and of Figure 5, in which a radius of 4 nm was used. Lipid/area calculation was obtained by dividing the total number of lipid molecules by the total area of the annulus. The same calculation was used to calculate the number of molecules dissolved in the bilayer in the setup “dissolution”, but counting only the lipid molecules within a radius of 8 nm from the center of the seipin ring.
In the systems containing seipin, the accumulation of TG molecules as a function of distance from the center of the seipin ring was calculated by counting the number of lipid molecules in annuli delimited by concentric circles of radius=R+1 nm, over the last 200 ns of simulation. The curves in Figure 4C (“ER-like” composition) have been further normalized by dividing the obtained values by the average number of lipids (PE, DG) per nm2 in the entire bilayer.
For the analysis of the contacts between the protein and TG molecules, the number of contacts between each residue of the protein and the glycerol bead of TG were calculated using the software GROMACS(19). A contact was defined when the distance between TG and the protein is lower than 0.6 nm. The number of contacts for corresponding residues in different monomers was summed and the final values are normalized by the length of the simulations. Only the contacts in the last 1 μs, when the simulation is at equilibrium, were used for the analysis.
The number of contacts between the protein and TG was calculated with the same criterium described above. The percentage of TG-TG contacts interacting inside the ring of seipin was obtained by subtracting the number of protein-TG contacts to the number of TG molecules inside the protein (radius of distance from the seipin center <=8 nm). Only the contacts for the last 2 μs of simulation are averaged.
Trajectories of single molecules for Figure 2G were obtained extracting the coordinates of TG molecules via the tool MDtraj(20) and used to plot the time evolution of the trajectory of the molecules and to compute the mean squared displacement.
For the calculation of the events in/out of the seipin ring, the coordinates of TG molecules from 3 μs of trajectory from different systems were extracted using the tool MDtraj and processed to count events. A buffer region with a radius between 6 and 8 nm from the seipin center was defined and an “in”-event was considered only if a TG molecule moved from a region of radius > 8 nm to a region of radius < 6 nm from the seipin center, or vice-versa for “out”-events.
To visualize the effect of different bilayer compositions and of seipin on bilayer curvature, we first aligned all systems so that the center of mass of the phospholipids is at {0,0,0}, and we then represented the head group of the phospholipids based on their z position (red: negative values, white = 0, blue: positive values).
All results in figures S1 and S5 are represented as average and standard deviation of the two independent replicas. For the “dissolution” systems, only one replica was run. For all the other systems, the results are represented as an average of the two independent replicas and the shaded regions correspond to the area between the curves of the two independent replicas. For the results in figure 2C inset and 3H, the error bars correspond to the difference between the two replicas and the average of the two.
All the images are rendered using VMD(14). The calculation of the number of TG molecules per distance from the protein seipin were performed using a tcl script, while the rest of analysis and graphs were produced using python scripts.

Experiments in human cells

Site directed mutagenesis. For site directed mutagenesis, PCRs were performed using high-fidelity Thermococcus kodakaraensis (KOD) HotStart DNA polymerase (Merck Millipore) with primers listed below:

F S165A S166A	ATGCTGGACACACTGGTCTTCgctgcgCTCCTGCTATTTGGCTTTGCA
R S165A S166A	TGCAAAGCCAAATAGCAGGAGcgcagcGAAGACCAGTGTGTCCAGCAT

Briefly, two PCR reactions were performed containing either forward or reverse primers. Following this, the PCR products were combined and a second PCR reaction was performed. Methylated DNA were digested using DpnI and clones were screened by Sanger sequencing.

Immunofluorescence. For immunofluorescence of HA-tagged Seipin, cells were transfected with vector or Seipin constructs for 48 hours. After 15 mins of oleic acid (OA) treatment, cells were washed with PBS and fixed with 4% PFA in PBS for 15 mins. After fixation, cells were permeabilized for 15 min with 0.2% Triton X-100 in PBS. Cells were then blocked with 3% BSA in PBS for 1 hr, followed by incubation with HA (#3274, Cell Signalling Technology) primary antibody diluted in blocking solution. Cells were washed three times in PBS, and incubated with Alexa Flour 594 secondary antibody (Invitrogen). Cells were washed three times with PBS and LDs were stained with BODIPY493/503 (Thermo Fisher Scientific). Finally, cells were mounted in ProLong Gold antifade reagent (Invitrogen).

Statistical analysis. Results are presented as mean ± standard deviation. n= 35 cells. Statistical analyses of results were performed using one-way ANOVA. Statistically significant differences are denoted as follows: ns $p > 0.05$, ****$p < 0.0001$.

Experiments in yeast cells

Yeast strains, media and growth conditions. Yeast strains and their genotype are listed in supplementary Table S3. Yeast strains were cultured in YP-rich medium [1% bacto yeast extract, 2% bacto peptone (USBiological, Swampscott, MA)] or selective (SC) medium [0.67% yeast nitrogen base without amino acids (USBiological), 0.73 g/l amino acids)], containing either 2% glucose or 2% galactose.

Yeast expression constructs. Plasmid YPlac111, a gift from R. Yang, University of South Wales, Australia, containing the yeast MET3 promoter was used as a backbone to express wild-type seipin and the mutant versions S165A/S166A and S165L/S166L fused to GFP. The plasmid was linearized with SphI and BamHI, and a PCR fragment containing seipin-GFP, S165A/S166A-GFP and S165L/S166L-GFP was inserted by homologous recombination in yeast(21), resulting in YPlac111-Seipin-GFP, YPlac111-S165A/S166A-GFP and YPlac111- S165L/S166L -GFP, respectively. All constructs were verified by sequencing (Microsynth AG, Buchs, Switzerland).

Western blot analysis. Cells corresponding to 3 OD600 units were harvested from an overnight culture in SC-media. Cells were incubated with NaOH, and proteins were precipitated using TCA and resuspended into sample buffer(22). Proteins were separated using SDS-PAGE and detected using a monoclonal antibody against GFP (mouse, 1: 2,000 dilution, no. 11814460001; Roche Diagnostics) or Pgk1 (mouse, 1:5,000 dilution; InvitrogenTM, no. 459250) and goat anti–mouse IgG (H+L)-HRP conjugates (1:10,000 dilution, no. 1706516; Bio-Rad). Subsequent detection occurred via peroxidase-coupled secondary antibodies and ECL Prime chemiluminescence substrate (Sigma-Aldrich) using an Image- Quant LAS 1000 biomolecular imager (GE Healthcare) and ImageQuant software. Western blot experiments were performed twice with similar results.

Fluorescence microscopy. Yeast cells were grown to early logarithmic phase (~1 OD600nm), pelleted by centrifugation and resuspended in SC galactose media. Images were acquired after 5,

15, 30 and 60 minutes of induction. At each time point, 3 µl of the cell suspension were mounted on a glass slide and covered with an agarose patch. Localization of mCherry- and GFP-tagged fusion proteins was performed by fluorescence microscopy of live yeast cells using a Visitron spinning disc CSU-W1 (Visitron Systems, Puchheim Germany). The Visitron spinning disk CSU-W1 consisted of a Nikon Ti-E inverted microscope, equipped with a CSU-W1 spinning disk head with a 50-µm pinhole disk (Yokogawa, Tokyo, Japan), an Evolve 512 (Photometrics) EM-CCD camera, and a PLAN APO 100x NA 1.3 oil objective (Nikon). Single plane images are displayed. Brightness and contrast were adjusted using Image J software and then resized in Photoshop (Adobe, Mountain View). Microscope experiments were performed on three different clones with essentially similar results. Counting of LD was performed manually in 100 cells for each time point.

Statistical analysis. Results are presented as mean ± standard deviation. Statistical analyses of results were performed using student T-test. Statistically significant differences are denoted as follows: ns $p > 0.05$, *$p < 0.05$. All the results are statistically significant against fld1Δ.

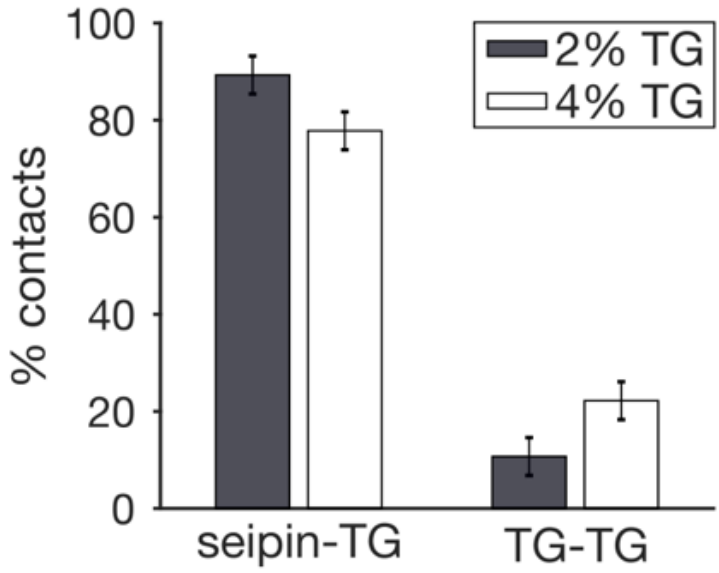

Fig. S1. Percentage of seipin-TG or TG-TG contacts in simulations at different TG concentrations.

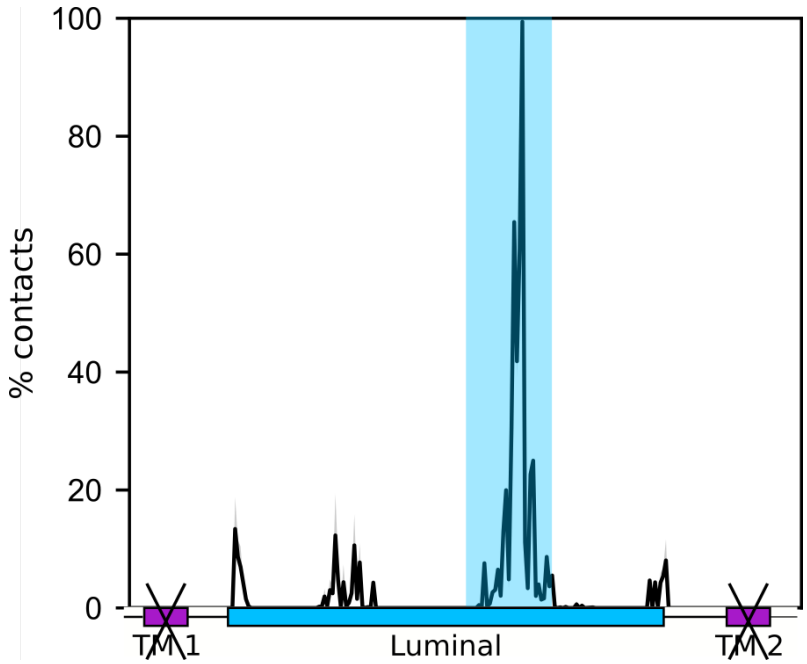

Fig. S2. Percentage of contacts between the luminal part of seipin and TG in simulations containing only the luminal domain of seipin.

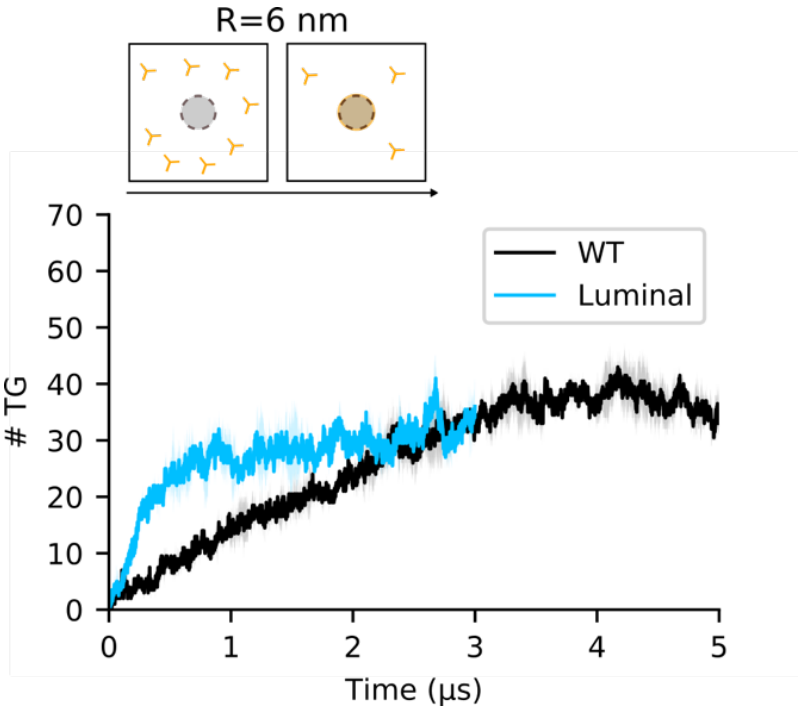

Fig. S3. Number of TG molecules inside the inner part of the seipin ring (R= 6 nm) over time during MD simulations of the luminal domain of seipin.

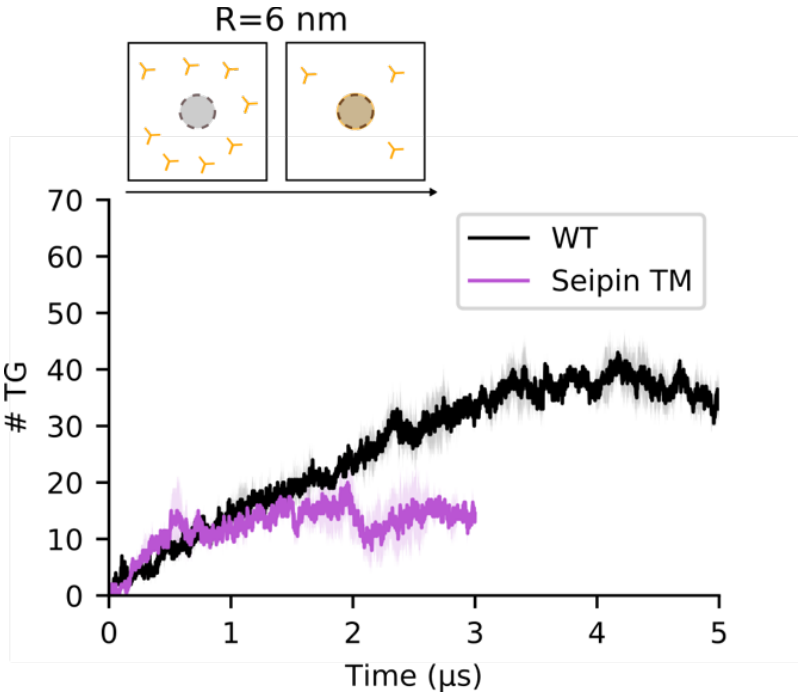

Fig S4. Number of TG molecules inside the inner part of the seipin ring (R= 6 nm) over time during MD simulations of the TM domains of seipin.

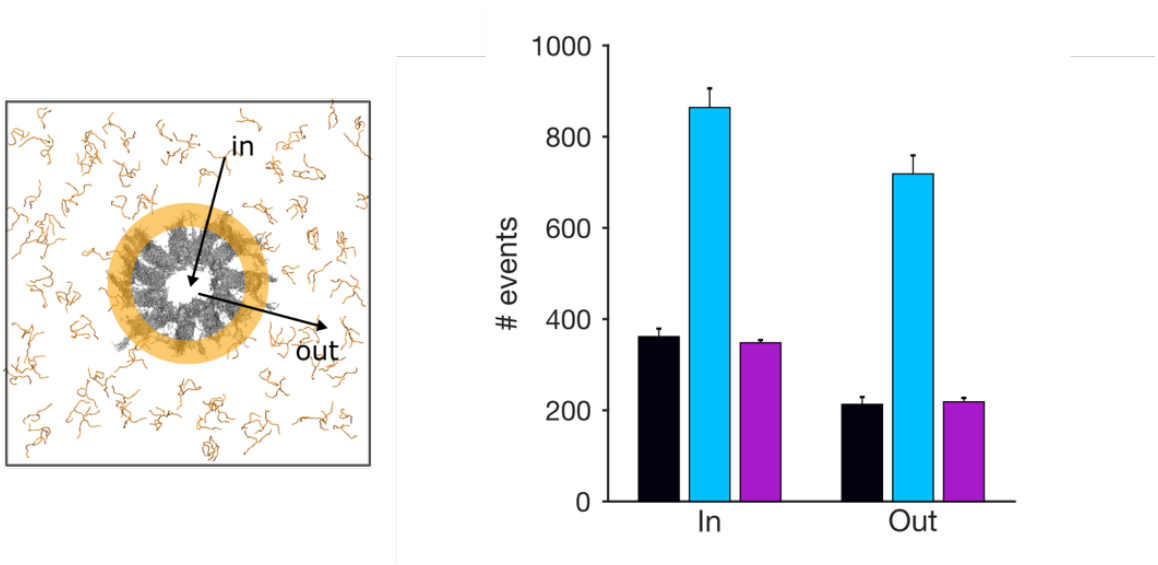

Fig S5. Number of events of molecules entering inside (in) or going outside (out) the seipin ring. The buffer region is colored in orange (see SI Appendix, Simulation analysis section).

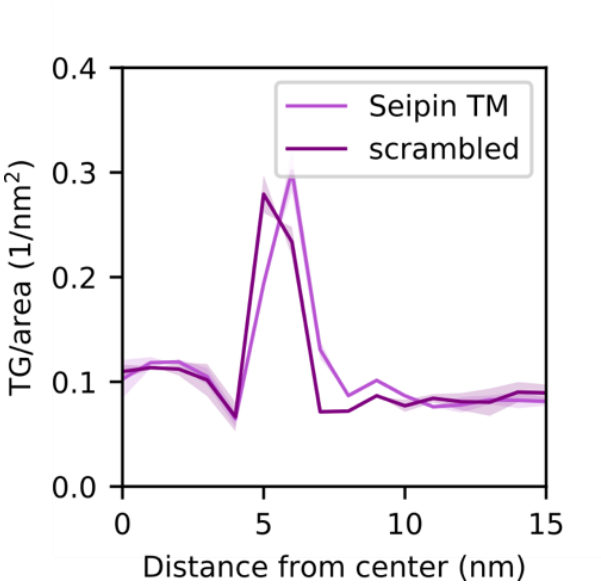

Fig S6. Radial distribution of TG molecules around seipin TM in MD simulations with "WT" TMs or scrambled TMs.

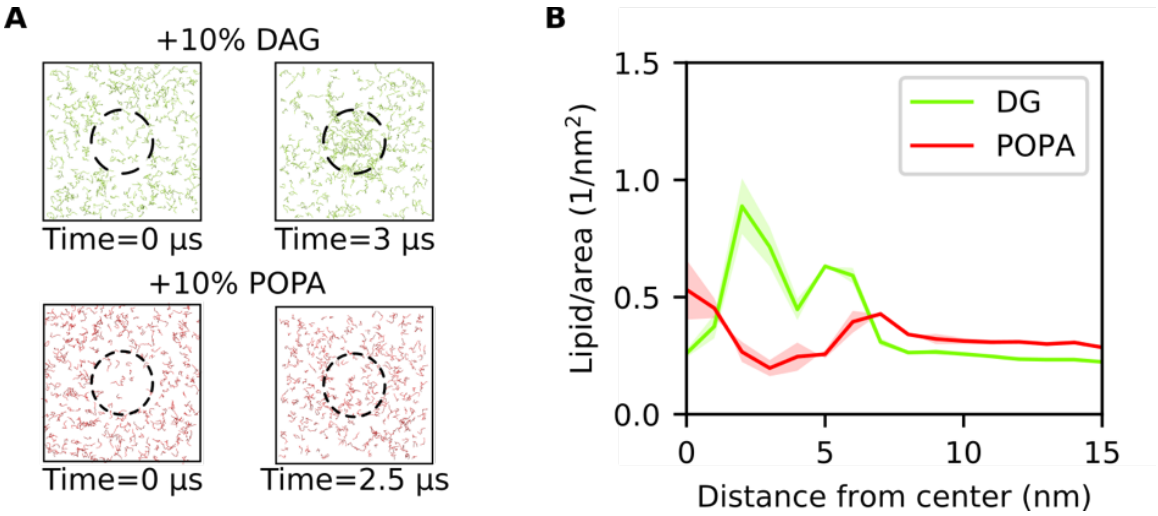

Fig S7. (A) Top view of systems containing DG or POPA at the beginning and at the end of the simulations. (B) Radial concentration of TG molecules in simulations of seipin with DG (green) or POPA (red).

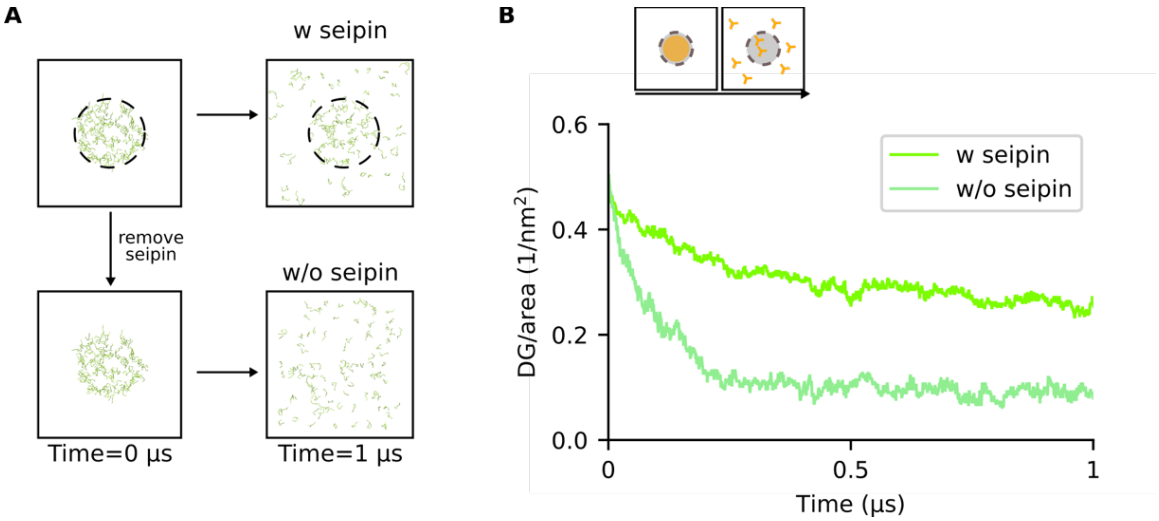

Fig S8. (A) Top view of initial and final snapshots of MD simulations of dissolution of DG blister with (top) and without (bottom) seipin. (B) Time evolution of the number of DG molecules inside the seipin ring when DG molecules are completely depleted from the surrounding lipid bilayer in the presence of the TM helices of seipin.

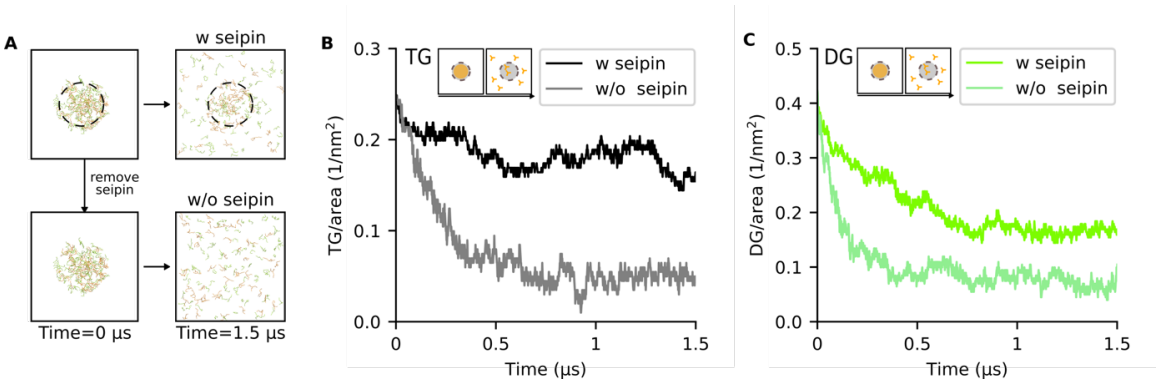

Fig S9. (A) Top view of initial and final snapshots of MD simulations of dissolution of DG/TG blister with (top) and without (bottom) seipin. (B) Time evolution of the number of TG molecules inside the seipin ring when DG and TG molecules are completely depleted from the surrounding lipid bilayer in the presence of the TM helices of seipin. (C) Time evolution of the number of DG molecules inside the seipin ring when DG and TG molecules are completely depleted from the surrounding lipid bilayer in the presence of the TM helices of seipin.

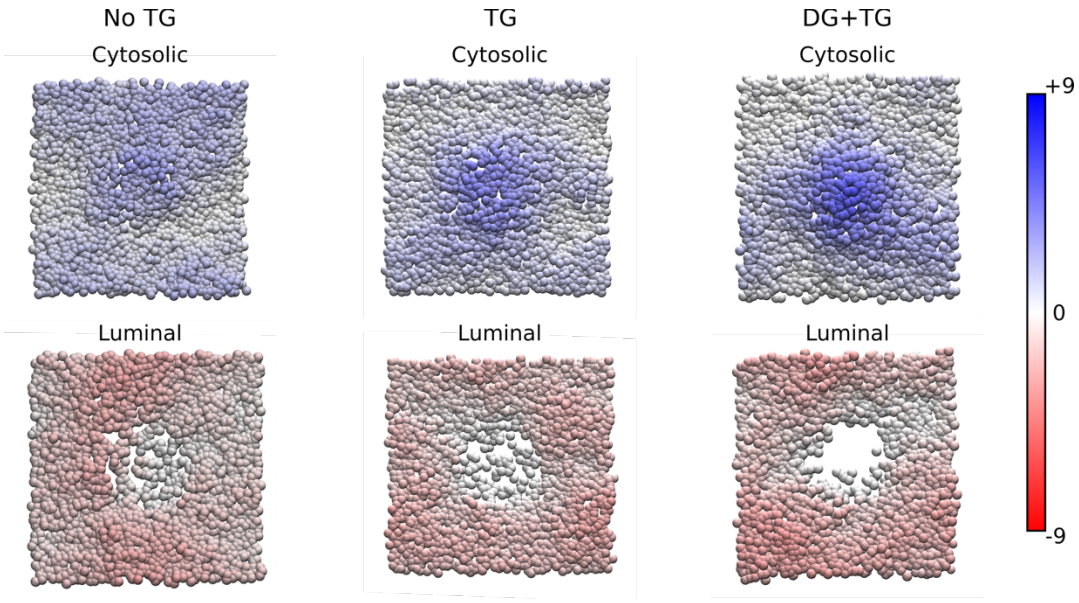

Fig S10. Top views of equilibrated snapshots of cytosolic and luminal leaflet in different systems (no TG, TG, DG+TG). The colors represent the position of the DOPC headgroups along the z direction (perpendicular to the membrane plane). Distances in the color scale are expressed in nm.

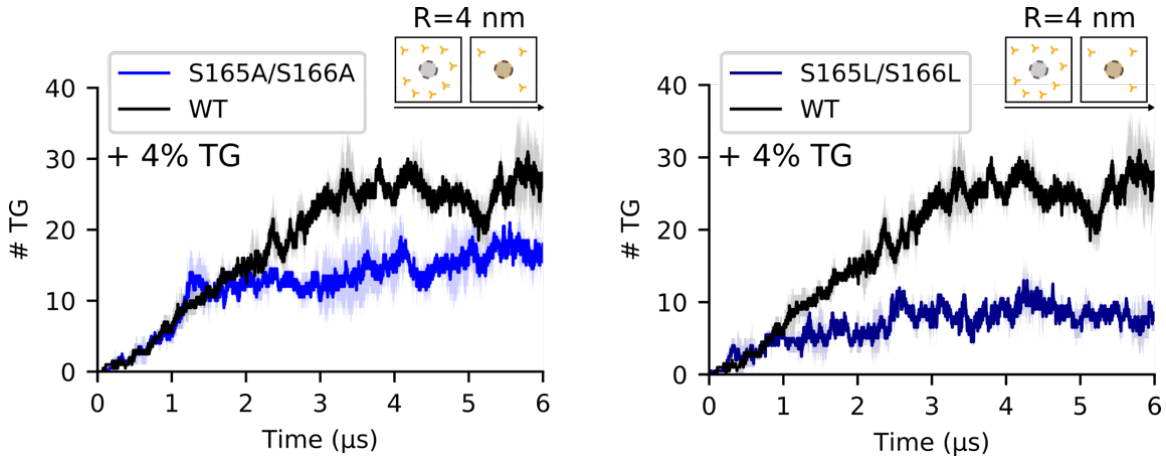

Figure S11. Number of TG molecules inside the part corresponding to the HH of the seipin (R= 4 nm) over time with WT protein or mutants, at 4% TG. Both WT and mutants are composed of TM, loops and luminal domain.

Table S1. List of all the *in silico* mutations.

Mutation name	Mutated residues/sequence	System
S165A/S166A	S165A, S166A	Luminal
S165L/S166L	S165L, S166L	Luminal
S165A/S166A	S165A, S166A	Entire
S165L/S166L	S165L, S166L	Entire
4polarL	S253L Y254L M255L Q256L	Helices
Scrambled	TM1: VLLFLGILFFLVVWSQLCTLL TM2: VQISYGMFLGFSTLIWWVWVF	Helices
$KALP_{21}$	TM1 and TM2 substituted with KALP21: $GKK(LA)_7LKKA$	Helices

Table S2. Details of the molecular simulations presented in this work. The abbreviation "WT" denotes the presence of the WT entire seipin protein in the system, "L" of only the luminal part, "H" of only the TM region, "E" of mutants with the entire structure (TMs + loops + luminal).

Bilayer composition (# of molecules)	TG molecules	# of replicas	Length (μs)
Accumulation			
3200 DOPC	64	1	7
3200 DOPC	128	1	7
28773 DOPC + WT (big)	545	1	2.5
28492 DOPC + WT (big)	1704	1	0.3
3281 DOPC + WT	110	2	7
3281 DOPC + WT	57	2	7
3368 DOPC + L	110	2	3
3368 DOPC + L	32	2	4
3357 DOPC + H	115	2	3
2576 DOPC + 310 DOG + WT	0	2	3
2576 DOPC + 310 DOG +WT	110	2	7
2911 DOPC + 344 POPA +WT	0	2	2.5
1884 DOPC + 970 DOPE +190 CHOL + 192 DOG +WT	57	2	3.5
Dissolution			
2576 DOPC + 95 DOG + WT	45	1	1.5
2576 DOPC + 95 DOG	45	1	1.5
2756 DOPC+125 DOG + WT	0	1	1
2756 DOPC+125 DOG	0	1	1
3661 DOPC +WT	36	1	2
3661 DOPC	36	1	2
2771 DOPC + H	54	1	1.7
2771 DOPC	54	1	1.7
Mutations			
S165A/S166A L + 3368 DOPC	32	2	4
S165L/S166L L + 3368 DOPC	32	2	4
S165A/S166A E + 3281 DOPC	110	2	6
S165L/S166L E + 3281 DOPC	110	2	6
4polarL H + 3357 DOPC	115	2	3
Scrambled H + 3357 DOPC	115	2	3
KALP H + 3357 DOPC	115	2	3

Table S3. *S. cerevisiae* strains used in this study.

Strain	Relevant Genotype	Source
RSY 6249	Matα his3Δ1 leu2Δ0 lys2Δ0 ura3Δ0 met15 are1::KanMX are2::kanMX dga1:: Lox-HIS-Lox trp1::URA3 GAL-LRO1:: TRP1 Erg6-mCherry::HIS	Lab Collection
RSY 6918	Matα his3Δ1 leu2Δ0 lys2Δ0 ura3Δ0 met15 are1::KanMX are2::kanMX dga1:: Lox-HIS-Lox trp1::URA3 fld1:: ClonNAt GAL-LRO1::TRP1 Erg6-mCherry::HIS	This Study

SI References

1. S. Plimpton, Fast Parallel Algorithms for Short–Range Molecular Dynamics. *J. Comput. Phys.* **117**, 1–19 (1995).
2. W. Shinoda, R. DeVane, M. L. Klein, Multi-property fitting and parameterization of a coarse grained model for aqueous surfactants. *Mol. Simul.* **33**, 27–36 (2007).
3. C. M. Macdermaid, *et al.*, Molecular dynamics simulations of cholesterol-rich membranes using a coarse- grained force field for cyclic alkanes Molecular dynamics simulations of cholesterol-rich membranes using a coarse-grained force field for cyclic alkanes. *J. Chem. Phys.* **143**, 243144 (2015).
4. W. Shinoda, R. DeVane, M. L. Klein, Computer simulation studies of self-assembling macromolecules. *Curr. Opin. Struct. Biol.* **22**, 175–186 (2012).
5. A. Bacle, R. Gautier, C. L. Jackson, P. F. J. Fuchs, S. Vanni, Interdigitation between Triglycerides and Lipids Modulates Surface Properties of Lipid Droplets. *Biophys. J.*, 1417–1430 (2017).
6. P. Campomanes, V. Zoni, S. Vanni, Local accumulation of diacylglycerol alters membrane properties nonlinearly due to its transbilayer activity. *Commun. Chem.* **2**, 72 (2019).
7. S. Seo, W. Shinoda, SPICA Force Field for Lipid Membranes: Domain Formation Induced by Cholesterol. *J. Chem. Theory Comput.* **15**, 762–774 (2019).
8. R. Devane, W. Shinoda, P. B. Moore, M. L. Klein, A Transferable Coarse Grain Non-bonded Interaction Model For Amino Acids. *J. Chem. Theory Comput.* **5**, 2115–2124 (2009).
9. S. Nosé, A molecular dynamics method for simulations in the canonical ensemble. *Mol. Phys.* **52**, 255–268 (1984).
10. G. J. Martyna, D. J. Tobias, M. L. Klein, Constant pressure molecular dynamics algorithms. *J. Chem. Phys.* **101**, 4177–4189 (1994).
11. M. Parrinello, A. Rahman, Polymorphic transitions in single crystals: A new molecular dynamics method. *J. Appl. Phys.* **52**, 7182–7190 (1981).
12. W. Shinoda, M. Shiga, M. Mikami, Rapid estimation of elastic constants by molecular dynamics simulation under constant stress. *Phys. Rev. B* **69**, 134103 (2004).
13. R. Yan, *et al.*, Human SEIPIN Binds Anionic Phospholipids. *Dev. Cell* **47**, 248-256.e4 (2018).
14. W. Humphrey, A. Dalke, K. Schulten, VMD: Visual Molecular Dynamics.
15. L. Martínez, R. Andrade, E. G. Birgin, J. M. Martínez, Packmol: A Package for Building Initial Configurations for Molecular Dynamics Simulations (2009) https:/doi.org/10.1002/jcc.21224.
16. A. Fiser, A. Sali, ModLoop: automated modeling of loops in protein structures. *Bioinformatics* **19**, 2500–2501 (2003).
17. S. Jo, T. Kim, V. G. Iyer, W. Im, CHARMM-GUI: A web-based graphical user interface for CHARMM. *J. Comput. Chem.* **29**, 1859–1865 (2008).
18. S. Jo, *et al.*, "CHARMM-GUI PDB manipulator for advanced modeling and simulations of proteins containing nonstandard residues" in *Advances in Protein Chemistry and Structural Biology*, (Academic Press Inc., 2014), pp. 235–265.
19. M. J. Abraham, *et al.*, GROMACS: High performance molecular simulations through multi-level parallelism from laptops to supercomputers. *SoftwareX* **1**–**2**, 19–25 (2015).
20. R. T. McGibbon, *et al.*, MDTraj: A Modern Open Library for the Analysis of Molecular Dynamics Trajectories. *Biophys. J.* **109**, 1528–1532 (2015).
21. S. bing Hua, M. Qiu, E. Chan, L. Zhu, Y. Luo, Minimum length of sequence homology required for in vivo cloning by homologous recombination in yeast. *Plasmid* **38**, 91–96 (1997).
22. A. Horvath, H. Riezman, Rapid protein extraction from Saccharomyces cerevisiae. *Yeast* **10**, 1305–1310 (1994).